Int. J. Electrochem. Sci., 6 **(2011)** 4329 - 4340

International Journal of
ELECTROCHEMICAL
SCIENCE
www.electrochemsci.org

Spherical Tin Oxide, SnO_2 Particles Fabricated via Facile Hydrothermal Method for Detection of Mercury (II) Ions

H.N. Lim [1,*], *R. Nurzulaikha* [2], *I. Harrison* [2], *S.S. Lim*[2], *W.T. Tan* [3], *M.C. Yeo* [3]

[1] Centre for Ionics University of Malaya, Physics Department, Faculty of Science, University of Malaya, 53400 Kuala Lumpur, Malaysia.
[2] Faculty of Engineering, The University of Nottingham Malaysia Campus, Jalan Broga, 43500 Semenyih, Selangor, Malaysia.
[3] Chemistry Department, Faculty of Science, Universiti Putra Malaysia, 43600 Serdang, Selangor, Malaysia.
[*]E-mail: janet_limhn@yahoo.com.my

Received: 13 July 2011 / *Accepted:* 15 August 2011 / *Published:* 1 September 2011

Smooth-surface spherical tin oxide particles were fabricated via hydrothermal processing route. X-ray diffraction (XRD) revealed that the particles consisted of the rutile phase of SnO_2 with tetragonal structure. The spherical morphology was realized with the aid of ammonia. The aggregation of SnO_2 particles could be avoided by adjusting the concentration of tin (II) chloride. Bare glassy carbon electrode (GCE) was modified with the hydrothermally prepared SnO_2 particles to detect the presence of mercury (II) ions (Hg^{2+}), in the presence of potassium chloride (KCl) as a supporting electrolyte. GCE modified with the spherical SnO_2 particles that possessed small crystallite size and smooth surface exhibited significantly enhanced oxidative and reductive current of Hg^{2+} during cyclic voltammetry compared with its bare counterpart. The reductive current was observed to increase by two fold and the detection limit of 75 nM for Hg^{2+} was achieved. This suggests that SnO_2 particles are a promising chemical sensor for the detection of Hg^{2+} in natural waters.

Keywords: Detection Limit, Hydrothermal, Mercury, Tin Oxide, Voltammetry

1. INTRODUCTION

Tin oxide is an n-type semiconductor with a large band gap of 3.6 eV [1]. SnO_2 is widely reported because it is very stable, has got high carrier density and supports enormous concentration of intrinsic and stoichiometry-violating vacancies, which is correlated to its electrical conductivity [2]. It has a wide range of applications as optoelectronic devices, dye-based solar cells, catalysts, gas sensors, electrochromic devices and electrode materials [1-4]. Though SnO_2 particles are widely applied for gas

sensing application due to their high mobility of conduction electrons, good chemical and thermal stability under the operating conditions of sensors [5], this material has rarely been envisaged as a chemical sensor for heavy metal ions in an aqueous condition.

A variety of techniques have been employed to synthesize small-sized tin oxide particles as miniaturization gives rise to unusual optical, electronic and chemical properties, and wide potential uses as devices [6]. These techniques include sol-gel, chemical vapour deposition, physical vapour evaporation, annealing precursor powders, thermal evaporation, thermal oxidation, microwave irradiation, anodic oxidation, homogeneous precipitation, spray pyrolysis, sputtering, pulsed laser deposition, solvothermal and hydrothermal [1, 5-7].

Of all the methods, hydrothermal route is much preferred for its simplicity and controllability of grain size, morphology and degree of crystallinity by changing the experimental parameters [5]. Moreover, it has been recognized as an environmentally friendly process because it uses water as a reaction medium and reaction is carried out in an autoclave, which is an enclosed system [8-10]. Hydrothermal method has been employed since the end of the 19th century, mainly in the production of synthetic minerals to imitate natural geothermal processes [11].

Mercury is one of the most toxic heavy metals known to organisms and the environment as even a trace amount of the element is potentially disastrous when ingested [12, 13]. The United Nations Environmental Programme (UNEP) estimated that an annual release of mercury was 4400 and 7500 metric tonnes [14] as a result of natural sources and human activities respectively [15], which contaminates the food chain and the environment.

The mercury limits for wastewater discharge and drinking water established by the World Health Organization (WHO), Environmental Protection Agency (EPA) and Ministry of the Environment of Japan are 5 – 10 μgL^{-1} (ca. 25 - 50 nM) and 0.5 – 2 μgL^{-1} (ca. 2.5 – 10 nM), respectively [16].

A popular method that has been developed for the detection of heavy metals is voltammetry because it allows the construction of sensitive voltammetric sensors that are specific/selective towards the chosen elements [17]. Voltammetric determination of mercury (II) ions (Hg^{2+}) in aqueous media using modified glassy carbon electrode (GCE) with organic molecules had detection limits ranging from 25 nM for cyclic voltammetry (CV) [18], 4 – 23 nM for linear sweep voltammetry (LSV) to 0.15 – 0.04 nM for differential pulse voltammetry (DPV) detection techniques [19]. The relatively low detection limits are crippled by complex and tedious synthesis and purification processes of organic molecules.

In this work, we fabricated tin oxide particles via facile hydrothermal method, in which acidified tin (IV) chloride was used as a precursor. We tuned the morphology of tin oxide by adjusting the concentrations of tin chloride, hydrochloric acid and ammonium hydroxide. GCE modified with the as-prepared tin oxide particles demonstrated promising results for the detection of Hg^{2+} using CV detection technique, indicating tin oxide particles' potential to be used as a chemical sensor in natural waters.

2. EXPERIMENTAL

2.1 Materials

Tin (IV) chloride pentahydrate ($SnCl_4.5H_2O$, 98%) and ammonia solution (NH_3, ~25%) were purchased from R&M Chemicals. Hydrochloric acid (HCl, 37%) and sodium chloride (NaCl, 99.5%) were purchased from Merck. Sodium hydroxide (NaOH, 99.99%), potassium chloride (KCl, 100%) and mercury (II) chloride ($HgCl_2$, 98%) were purchased from HmbG Chemicals, J. T. Baker and Fischer General Scientific, respectively. Distilled water was used throughout the sample preparation.

2.2 Synthesis of tin oxide powder

15 ml of 0.7 M of $SnCl_4.5H_2O$ solution, acidified with 1 M of HCl solution, was mixed with 6 ml of 0.01 M of NH_4OH solution. The mixture was homogenized for 5 min for a complete dissolution and poured into a teflon-lined autoclave. The autoclave was placed in an oven at 160 ^oC for 4 h. The resulting white precipitate was centrifuged, washed with copious amount of water and dried at 60^oC for 24 h. Samples prepared with varying concentrations and reaction times are shown in Table 1. Conventional chemical precipitation method was used to prepare bulk tin oxide powder, which is yellow in colour, whereby 0.4 M of $SnCl_4.5H_2O$ was titrated with 2 M of NaOH while stirring until precipitation occurred.

2.3 Characterization

The crystalline phase was determined using a Phillip X-ray diffractometer (XRD) employing a scanning rate of $0.033^o s^{-1}$ in a 2θ range from 20^o to 70^o with Cu Kα radiation (λ = 1.5418 Å). Field emission scanning electron microscopy (FESEM) images were obtained on a FEI CU200 scanning electron microscope operated at 10.0 kV.

2.4 Cyclic Voltammetry

A Model BAS 50W electrochemical analyzer from Bioanalytical System Inc. USA was used for cyclic voltammetry (CV) study. It was equipped with an electrochemical cell that consists of three electrodes, which were a glassy carbon electrode (GCE, 3 mm in diameter) as working electrode, an Ag/AgCl (in 3 M NaCl) as reference electrode and a platinum wire as counter electrode. Before modification, the bare GCE was polished to a mirror-like appearance with alumina slurry on micro-cloth pads, rinsed thoroughly with distilled water between each polishing step, then washed successively with distilled water and anhydrous alcohol. For preparation of modified electrode, the samples were introduced onto the bare GCE by tapping the GCE successively for ten times onto the samples [20]. 10 ml of 0.1 M of KCl as supporting electrolyte was pipetted into an electrochemical cell. 190 μl of 1.0 mM of $HgCl_2$ was used as analyte. Then, all the three electrodes were immersed into the supporting electrolyte solution. N_2 gas was bubbled into the solution for 15 min to remove the

dissolved oxygen before voltammogram was recorded. Potential range was checked before any readings on the voltammogram were recorded. All the voltammetric experiments were referred at ambient temperature of 25 ± 2 ^{o}C.

3. RESULTS AND DISCUSSION

Figure 1 shows the XRD patterns of the hydrothermally prepared tin oxide particles and tin oxide bulk. All the peaks in the patterns corresponded to the rutile phase of SnO_2 with tetragonal structure, which is indexed to JCPDS file no. 41-1445. No impurity peak was detected. Debye-Scherrer's equation is used to estimate average crystallite sizes of the hydrothermally prepared SnO_2 samples, using its (110) reflections [21]. The average crystallite sizes of A1, B1, C1, A2, B2, and C2 are 24.6 nm, 11.9 nm, 41.4 nm, 6.5 nm, 19.6 nm and 24.8 nm, respectively as displayed in Table 1. As compared to A1, reduction of precursor concentration reduced the peak intensities considerably and the diffraction peaks are broadened due to the small crystallite size as reflected in A2. Reduction of reaction time by half does not appear to affect the peak intensities as observed in B1 and B2. Although the absence of ammonia (NH_3) did not alter the phase and structure of SnO_2 as shown in C1 and C2, the reduction of precursor concentration in C2 did reduce the peak intensity, broaden the peak and reduce the crystallite size compared with C1. In fact, C1 has the most well-defined diffraction peaks, which is probably contributed by the absence of the residue of NH_3 molecules enveloping the crystallites.

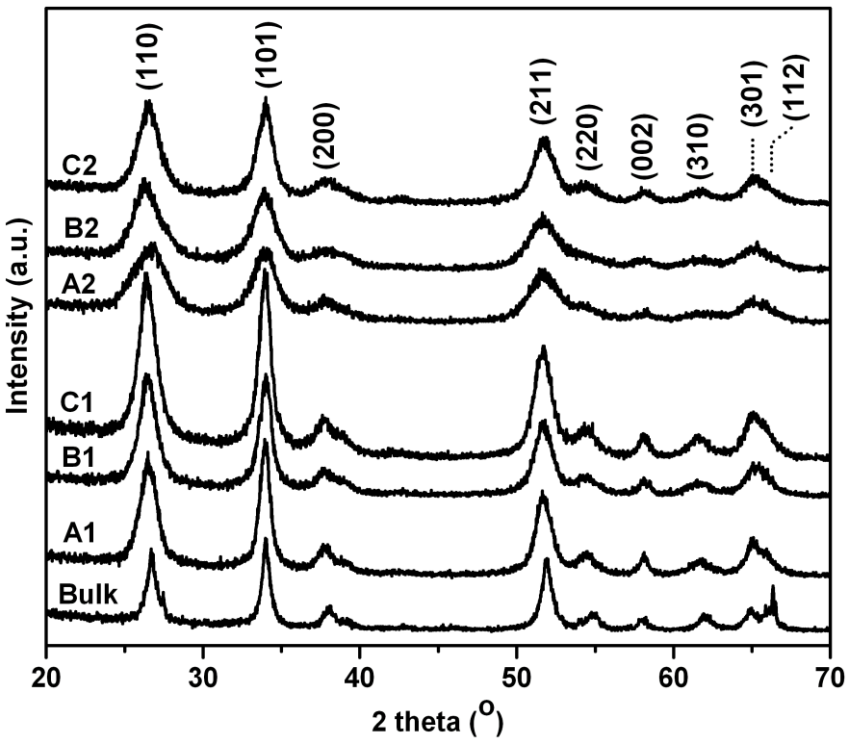

Figure 1. XRD patterns of SnO_2 bulk and particles.

Table 1. Synthesis parameters and crystallite size of tin oxide particles.

Sample	$SnCl_4.5H_2O$	HCI solution (M)	NH_4OH solution	Reaction time (h)	Crystallite size (nm)
A1	15 ml, 0.7 M	1.0	6 ml, 0.100 M	4	24.6
B1	15 ml, 0.7 M	1.0	6 ml, 0.100 M	2	11.9
C1	15 ml, 0.7 M	1.0	-	4	41.4
A2	15 ml, 0.5 M	0.5	6 ml, 0.100 M	4	6.5
B2	15 ml, 0.5 M	0.5	6 ml, 0.100 M	2	19.6
C2	15 ml, 0.5 M	0.5	-	4	24.8

Bulk SnO_2 particles prepared using conventional method have large dimension of approximately 50 μm as shown in Figure 2. While FESEM micrographs in Figure 3 display dramatic effects of hydrothermal processing route and concentration change of chemicals on the morphology of the samples. The particle sizes of the samples are not in agreement with the crystallite sizes calculated from the Debye-Scherrer's equation, which was due to the agglomeration of SnO_2 crystallites into micron-sized particles. As shown in Figure 3, A1 consists of micron-sized particles and observation at a higher magnification shows that the surface of A1 is rough, which indicates that the nanocrystallites of the sample had agglomerated into large particles. When the concentrations of tin chloride and hydrochloric acid were reduced, the particles became spherical and the surface became smoother as displayed by A2.

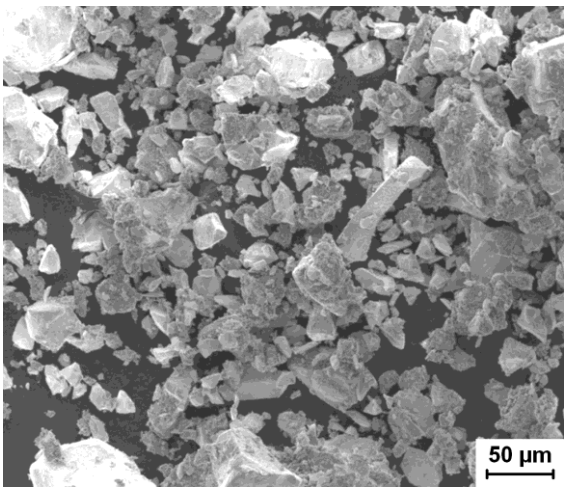

Figure 2. FESEM image of SnO_2 bulk prepared using non-hydrothermal method.

The roughness of the surface is in agreement with the crystallite sizes of the samples calculated from the Debye-Scherrer's equation, where the particles with rougher surface have larger crystallite size. Unlike concentration change of chemicals, reaction time had no effect on the morphology of the samples as they remained the same even after halving the reaction time as shown by B1 and B2. However, the surface of B2 is rougher than A2, as reflected in the crystallite size. The effect of NH_3

was investigated by removing it from the reaction. The absence of NH_3 yielded samples with irregular morphology as revealed under the FESEM observation for C1 and C2, which suggests that NH_3 molecules played an important role during the nucleation and growth of SnO_2. Moreover, the absence of NH_3 gave rise to increased surface roughness, which is reflected by the large crystallite sizes of C1 and C2 estimated from the XRD results. It is observed that the A1, B1 and C1 particles, which were prepared at a higher precursor concentration, have a higher degree of aggregation of particles compared with the A2, B2 and C2 particles, which were prepared at a lower precursor concentration.

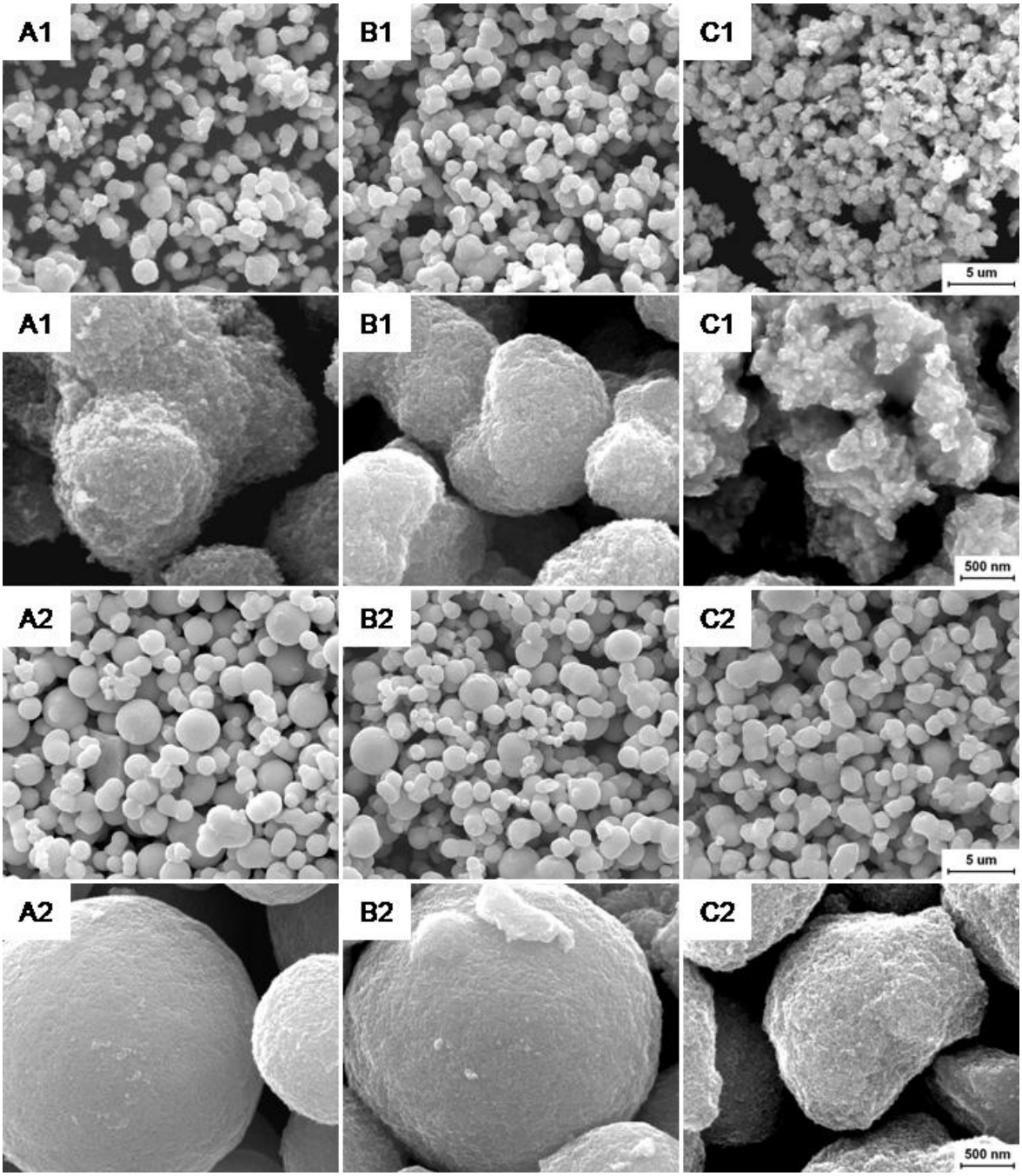

Figure 3. FESEM images of SnO_2 particles prepared via hydrothermal method. Each row of images shares the same scale bar.

The behaviour of NH_3 may correlate to a process called molecule recognition that could have taken place at the inorganic/organic interface due to charge and stereochemistry complementarity [22, 23]. In an aqueous system, NH_3 would ionize completely and result in a tetrahedral structure with lone pair electrons. Thus, tin cations could be incorporated to NH_3 by the charge as shown in Figure 4. A plausible mechanism for the templating process is that $H_3N\text{-}Sn^{4+}$ complexes formed micelles that contained many tin cations on the surface (Figure 5a). The micelles acted as nucleating points for the growth of SnO_2 crystals. During the hydrothermal stage, $H_3N\text{-}SnO_2$ complexes were produced (Figure 5b) and they coalesced to form a large particle (Figure 5c). Since the crystallization process was under the critical control of NH_3, the resulting particles were invariably spherical [24]. Aggregation of the micron-sized particles only occurred in the samples prepared at the higher precursor concentration (A1, B1 and C1) as NH_3 molecules were unable to fully envelope the particles while crystal growth took place. This observation is in agreement with our previous study that at high reactant concentration, crystal growth will lead to aggregated morphology, which is contributed by the Ostwald ripening process [25].

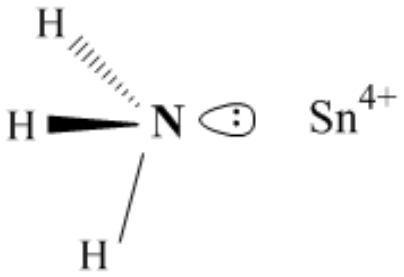

Figure 4. Schematic drawing of the complementarity between the lone pair electrons of NH_3 and tin cation.

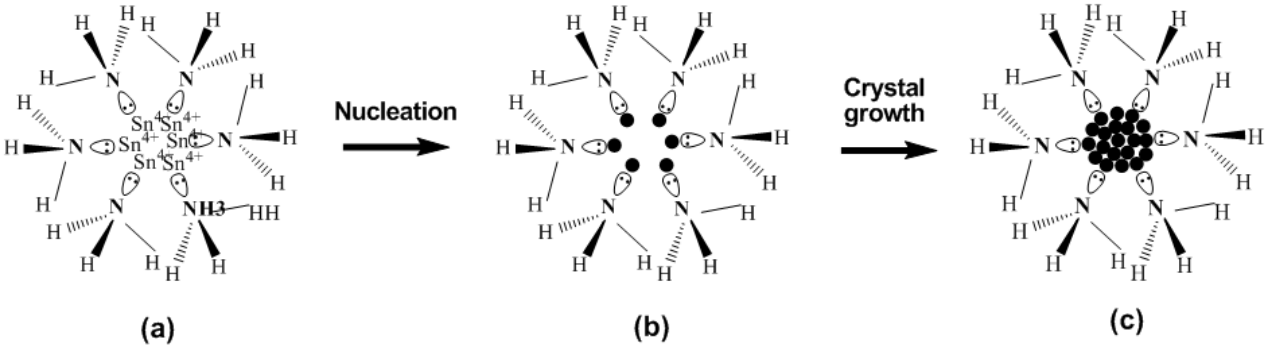

Figure 5. Formation mechanism of spherical SnO_2 particles.

The electrochemical performances of the samples, examined by cyclic voltammetry with a scan rate of 50 mV/s, are exhibited in Figure 6. The background current behavior for bare GCE in KCl supporting electrolyte is almost plateau for oxidizing and reducing reactions (blue line) as shown in Figure 6a. SnO_2 bulk modified GCE in KCl supporting electrolyte has a similar feature (purple line).

In contrast, the presence of mercury (II) ions (Hg^{2+}) in KCl supporting electrolyte resulted in a distinctive oxidizing peak current, which is observed between +0.1 V and +0.2 V (I) (red line) vs Ag/AgCl. SnO_2 bulk modified GCE in KCl supporting electrolyte spiked with Hg^{2+} enhanced the oxidative current by approximately 30 μA, in addition to the appearance of one small oxidative peak between -1.0 V and -0.8 V (II) and two reductive peaks between -0.3 and -0.1 V (III) and +0.3 and +0.6 (IV) (green line). All the peaks are most likely to arise through the stepwise reduction of Hg^{2+} + $e^- \leftrightarrows Hg^+$ and $Hg^+ + e^- \leftrightarrows Hg^0$.

In Figure 6b, the entire hydrothermally prepared SnO_2 modified GCE displays improved electrochemical performance, especially in the reducing reaction, than SnO_2 bulk. The reductive peak currents were enhanced, signifying increased sensitivity to the detection of Hg^{2+}. Moreover, all the peaks (I – IV) shifted to the 0.0 V potential, which indicates that electrocatalysis process had occurred [26]. There is also an appearance of a broad peak between -1.0 V and -0.7 V (V). B1 (green line) has the most enhanced electrochemical activity followed by A1 (red line) and C1 (purple line), in which the order of the crystallite size and surface roughness ascended in the same sequence. The electrochemical performances for the samples prepared at a lower precursor concentration was also affected by the crystallite size and surface roughness, whereby A2 (red line) with the smoothest surface exhibits significantly enhanced peak currents and electrocatalytic activity (Figure 6c). The electrocatalytic activity of C2 (purple line) is better than B2 (green line) up to the potential of -0.1 V where, thereafter, the peaks for B2 are slightly more enhanced than C2. This could be due to the small difference in crystallite size of the two samples. The redox process of Hg (II) was electrocatalyzed by every SnO_2 sample present on the SnO_2/GC electrode surface. Among all the samples, A2 possessed the best reducing reaction, which possibly makes it an efficient redox-recyclable material for the extraction of heavy element ions from waste water [27]. Based on the XRD, FESEM and electrochemical analyses, the small crystallite size and smooth surface of particles are beneficial for the enhancement of peak currents and electrocatalytic effect.

As A2 displays the best electrocatalytic activity with tremendously enhanced oxidative and reductive currents, we assessed the stability of A2 modified GCE by continuous potential cycling. Figure 7 shows that even though the current associated with oxidation and reduction of Hg^{2+} shifted downward after the twentieth potential cycle, the oxidation and reduction peaks of Hg^{2+} remained high, reflecting the stability of A2 coating. As the oxidative peak (I) is well-defined and remains unchanged during the cycles, even with increasing concentration of Hg^{2+} as shown in Figure 8a, it can thus be used to detect the concentration of Hg^{2+} in KCl supporting electrolyte. Figure 8b displays the points obtained from the peak current of Figure 8a, which was fitted polynomially. The inset of Figure 8b shows the calibration graphs of Hg^{2+} in the supporting electrolyte. Linear response was achieved over a concentration range of 0.5 μM to 10 μM. Based on the equation 3σ/slope, where σ is the standard deviation of the background noise of 50 data points adjacent to the oxidation peak of Hg^{2+}, a detection limit of 75 nM was determined. The detection limit for SnO_2 bulk was also determined following the same method and equation, leading to a value of 1000 nM, which was two order higher than A2. This indicates the importance of miniaturization for increased sensitivity towards the detection of Hg^{2+}.

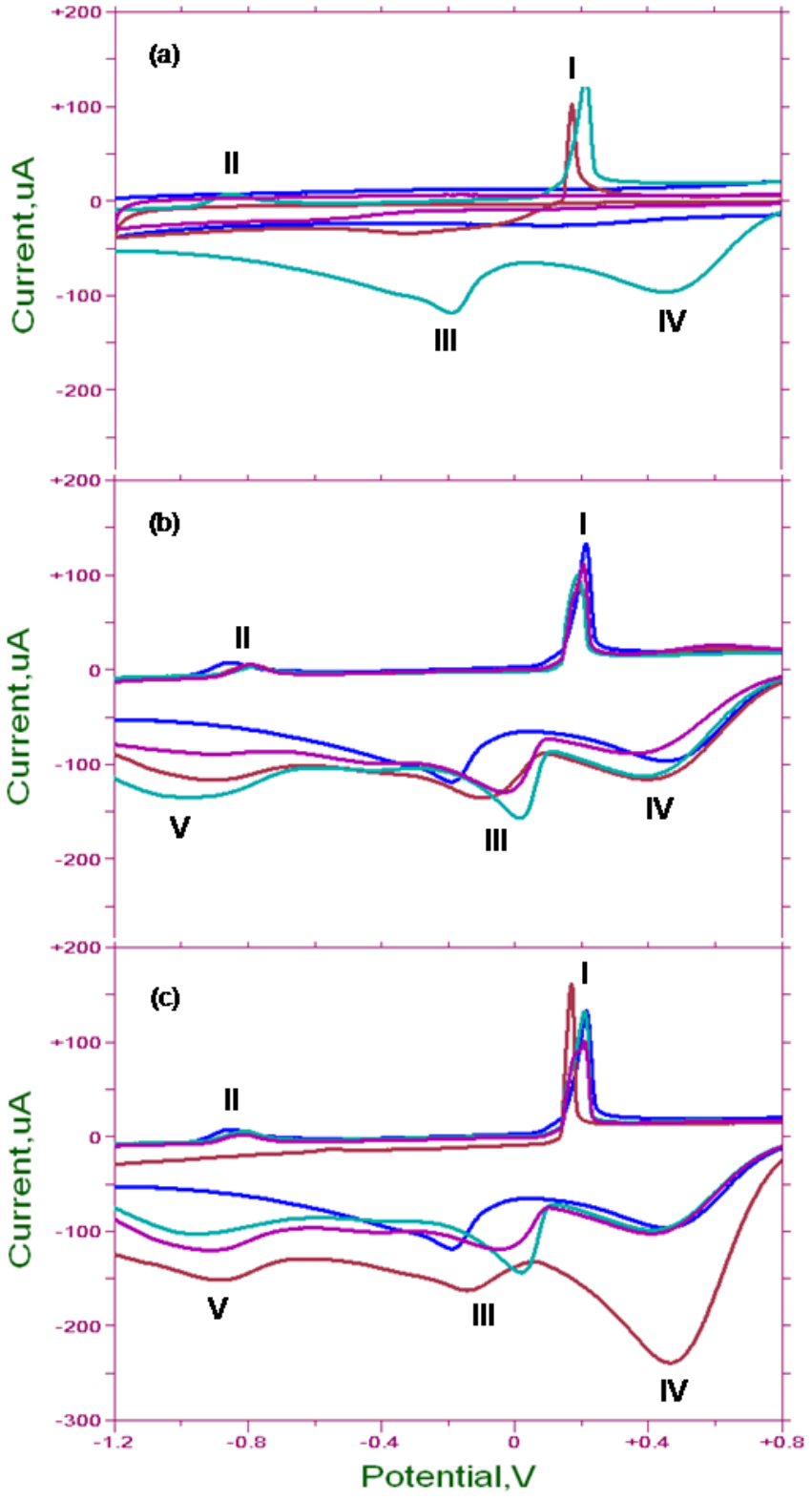

Figure 6. Electrochemical analysis of (a) bare GCE in KCl supporting electrolyte (blue line), SnO_2 bulk modified GCE in KCl supporting electrolyte (purple line), bare GCE in KCl supporting electrolyte and Hg^{2+} ionic solution (red line) and SnO_2 bulk modified GCE in KCl supporting electrolyte and Hg^{2+} ionic solution (green line); (b) SnO_2 bulk (blue line), A1 (red line), B1 (green line) and C1 (purple line) in KCl supporting electrolyte and Hg^{2+} ionic solution; and (c) SnO_2 bulk (blue line), A2 (red line), B2 (green line) and C2 (purple line) in KCl supporting electrolyte and Hg^{2+} ionic solution.

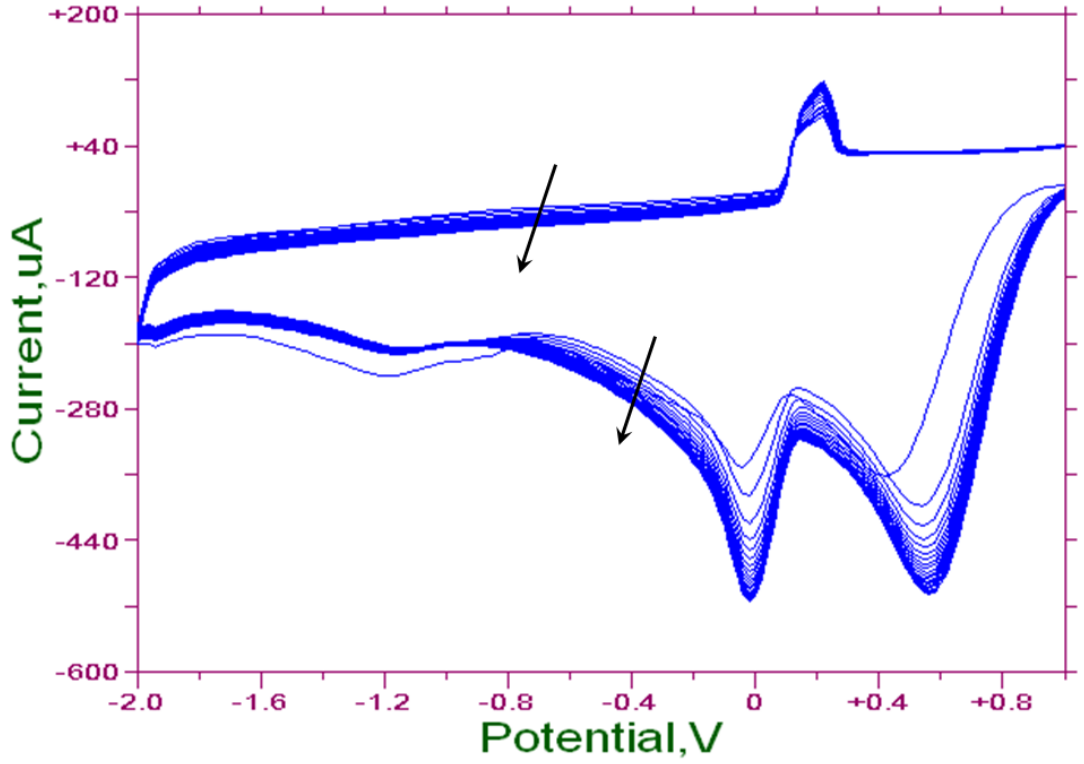

Figure 7. Multiple cyclic voltammetry of A2 modified GCE in 0.1 M of KCl supporting electrolyte and 1.0 mM of Hg^{2+} ionic solution. The two arrows indicate the current shifting downward.

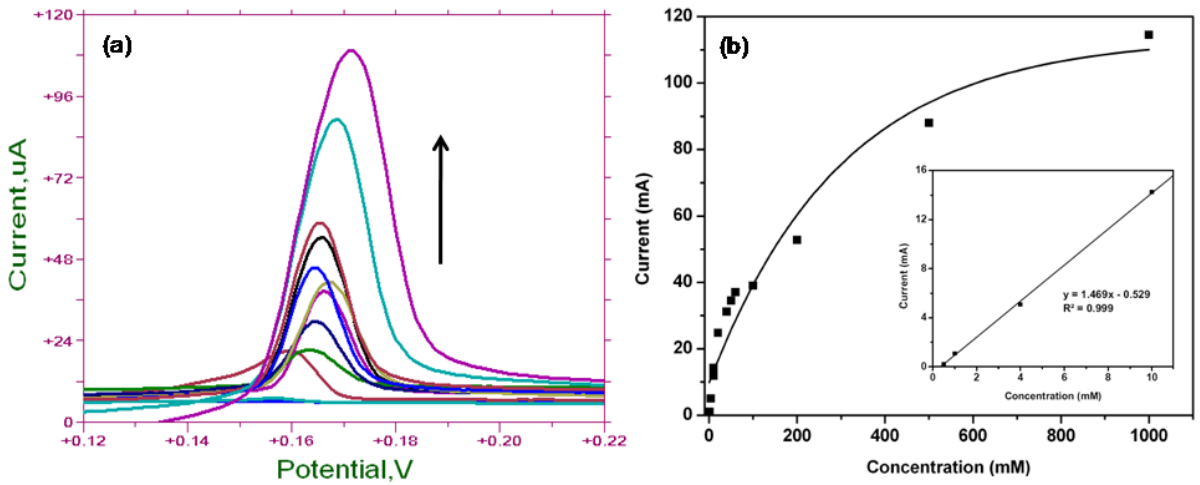

Figure 8. (a) Cyclic voltammograms of various concentrations of Hg^{2+} ionic solution. Arrow pointing upward indicates increasing concentration. (b) Polynomial graph of current-concentration and inset showing calibration graph of Hg^{2+} ionic solution.

4. CONCLUSION

The formation of spherical SnO_2 particles was strongly affected by the presence of NH_3 molecules and the concentration of tin (IV) chloride. Surface roughness of the samples was directly

correlated to the crystallite size of the metal oxide, which complemented the FESEM observation. Larger crystallite size gave rise to rougher surface particle. Spherical particles with smooth surface had better electrochemical performance evidenced from the increased oxidative and reductive current. The coating of the smooth surface spherical particles remained strongly and stably adhered to the GCE even after twenty times of potential cycling as manifested by the high oxidation and reduction peaks. The spherical SnO_2 particles modified GCE with a detection limit of 75 nM holds great promise for the determination of Hg^{2+} in aqueous media. Future development entails further downsizing SnO_2 particles to nanometer dimension, which could potentially reduce the detection limit of Hg^{2+}. The advantages of using SnO_2 as a modifying agent for GCE are the availability of the metal oxide, the economy feasibility, the facile synthesis method and the widely reported excellent properties, particularly the high mobility of conduction electrons.

ACKNOWLEDGEMENT

The authors gratefully acknowledge Dr. Huang N.M. of the Low Dimensional Materials Research Centre of the University of Malaya for his generous technical contributions. This work was supported by the High Impact Research Grants (UM.C/625/1/HIR/030 and UM.C/625/1/HIR/MOHE/05) and the University of Malaya Research Grant (RG096/10AFR).

References

1. Z. Li, W. Shen, X. Zhang, L. Fang, X. Zu, *Colloid Surface A* 327 (2008) 17.
2. S. Das, S. Chaudhuri, S. Maji, *J. Phys. Chem. C* 112 (16) (2008) 6213.
3. J. Ning, Q. Dai, T. Jiang, K. Men, D. Liu, N. Xiao, C. Li, D. Li, B. Liu, B. Zou, G. Zou, W.W. Yu, *Langmuir* 25 (3) (2008) 1818.
4. H. Wang, F. Sun, Y. Zhang, L. Li, H. Chen, Q. Wu, J.C. Yu, *J. Mater. Chem.* 20 (2010) 5641.
5. B.M. Matin, Y. Mortazavi, A.A. Khodadadi, A. Abbasi, A.A. Firooz, *Sensor Actuat. B - Chem* 151 (2010) 140.
6. M. Krishna, S. Komarneni, *Ceram. Int.* 35 (2009) 3375.
7. T.F. Baumann, S.O. Kucheyev, A.E. Gash, J.H. Satcher, *Adv. Mater.* 17 (2005) 1546.
8. A.Kawai-Nakamura, T. Sato, K. Sue, S. Tanaka, K. Saitoh, K. Aida, T. Hiaki, *Mater. Lett.* 62 (2008) 3471.
9. C. Lazau, L. Mocanu, I. Miron, P. Sfirloaga, G. Tanasie, C. Tatu, A. Gruia, I. Grozescu, *Digest J. Nanomater. Biostruc.* 2 (2007) 257.
10. K.M. Reddy, D. Guin, S.V. Manorama, A.R. Reddy, *J. Mater. Res.* 19 (2004) 2567.
11. Z. Fang, H. Assaaoudi, H. Lin, X. Wang, I.S. Butler, J.A. Kozinski, *J. Nanopart. Res.* 9 (2007) 683.
12. Y.M. Panta, J. Liu, M.A. Cheney, S.W. Joo, S. Qian, *J. Colloid Interf. Sci.* 333 (2) (2009) 485.
13. M. Yamamoto, T. Charoenraks, H. Pan-Hou, A. Nakano, A. Apilux, M. Tabata, *Chemosphere* 69 (4) (2007) 534.
14. J. Liu, Y. Lu, *Angew. Chem. Int. Edit.* 46 (2007) 7587.
15. H. Li, J. Zhai, J. Tian, Y. Luo, X. Sun, *Biosens. Bioelectron.* 26 (2011) 4656.
16. J. Zhu, B. Deng, J. Yang, D. Gang, *Carbon* 47 (2009) 2014.
17. P. Ugo, L.M. Moretto, G.A. Mazzocchin, *Anal. Chim. Acta* 305 (1-3) (1995) 74.
18. J. Lu, X. He, X. Zeng, Q. Wan, Z. Zhang, *Talanta* 59 (2003) 553.
19. P. Ugo, L.M. Moretto, G.A. Mazzocchin, *Anal. Chim. Acta* 305 (1995) 74.
20. A.M. Bond, F. Marken, *J. Electroanal. Chem.* 372 (1-2) (1994) 125.

21. N.M. Huang, S. Radiman, H.N. Lim, S.K. Yeong, P.S. Khiew, W.S. Chiu, G.H.M. Saeed, K. Nadarajah, *Chem. Eng. J.* 147 (2009) 399.
22. D.H. Gray, S. Hu, E. Juang, D.L. Gin, *Adv. Mater*. 9 (1997) 731.
23. D. Walsh, J.L. Kingston, B.R. Heywood, S. Mann, *J. Cryst. Growth* 133 (1993) 1.
24. Y. Wang, S. Zhang, K. Wei, N. Zhao, J. Chen, X. Wang, *Mater. Lett.* 60 (2006) 1484.
25. H.N. Lim, A. Kassim, N.M. Huang, R. Hashim, S. Radiman, P.S. Khiew, W.S. Chiu, *Ceram. Inter.* 35 (2009) 2891.
26. M. Zidan, W.T. Tan, Z. Zainal, A.H. Abdullah, J.K. Goh, *Int. J. Electrochem. Sci.* 5 (2010) 501
27. P.K. Dorhout, S.H. Strauss, *Inorg. Mater. Syn.* 727 (1999) 53